Edge Debonding in Peeling of a Thin Flexible Plate From an Elastomer Layer: A Cohesive Zone Model Analysis

Bikramjit Mukherjee[1]
Department of Biomedical Engineering and Mechanics, M/C 0219, Virginia Polytechnic Institute and State University, Blacksburg, VA 24061

Romesh C. Batra
Fellow ASME
Department of Biomedical Engineering and Mechanics, M/C 0219, Virginia Polytechnic Institute and State University, Blacksburg, VA 24061
e-mail: rbatra@vt.edu

David A. Dillard[2]
Fellow ASME
Department of Biomedical Engineering and Mechanics, M/C 0219, Virginia Polytechnic Institute and State University, Blacksburg, VA 24061
e-mail: dillard@vt.edu

A cohesive zone modeling (CZM) approach with a bilinear traction-separation relation is used to study the peeling of a thin overhanging plate from the edge of an incompressible elastomeric layer bonded firmly to a stationary rigid base. The deformations are approximated as plane strain and the materials are assumed to be linearly elastic, homogeneous, and isotropic. Furthermore, governing equations for the elastomer deformations are simplified using the lubrication theory approximations, and those of the plate with the Kirchhoff–Love theory. It is found that the peeling is governed by a single nondimensional number defined in terms of the interfacial strength, the interface fracture energy, the plate bending rigidity, the elastomer shear modulus, and the elastomeric layer thickness. An increase in this nondimensional number monotonically increases the CZ size ahead of the debond tip, and the pull-off force transitions from a fracture energy to strength dominated regime. This finding is supported by the results of the boundary value problem numerically studied using the finite element method. Results reported herein could guide elastomeric adhesive design for load capacity and may help ascertain test configurations for extracting the strength and the fracture energy of an interface from test data. [DOI: 10.1115/1.4034988]

Keywords: elastomeric interlayer, debonding, cohesive zone model (CZM), peeling

Introduction

The understanding of parameters that control and affect adhesive/interfacial debonding of sandwiched elastomeric layers is critical in numerous applications such as fabrication of soft ophthalmic lenses, optimizing transfer printing processes, ensuring durability of sealants, designing laminated safety glasses and biomimetic adhesives, as well as restricting fouling of barnacles on ship hulls. The mechanics of interfacial debonding of elastomer interlayers, especially the collective role played by the geometric and the material parameters, and the interfacial adhesion has been a subject of considerable interest for a long time.

Here, we analyze a prototype problem, namely, the peeling off of an overhanging flexible plate from an elastomer layer bonded firmly to a stationary rigid base. Previous studies on similar problems [1–4] that focused not necessarily on elastomer interlayers recognized the importance of the collective role of the flexural rigidity (D_p) of the plate, and Young's modulus (E) and the thickness (h) of the interlayer on the elastomer deformations and on the pull-off force required for peeling. For example, Bikerman [3] treated the interlayer as a Winkler elastic foundation, used a critical peel stress (T_c) as the debonding criterion, and found that the pull-off force per unit plate width (P_c) was given by $P_c \sim T_c(D_p h/E)^{1/4}$ where $(D_p h/E)^{1/4}$ quantifies the length scale of the peel stress oscillations decaying along the peeling direction. The coupling of a linear elastic fracture mechanics (LEFM) approach with the Winkler foundation analysis [5] predicts that $P_c \sim (D_p h/E)^{1/4}\sqrt{\mathcal{G}_c E/h}$ where $\mathcal{G}_c$ is the fracture energy of the interface. These studies approximated deformations of the interlayer as uniaxial stretching of independent strands (effective Poisson's ratio of zero). This assumption becomes especially erroneous for nearly incompressible elastomers. The state of hydrostatic stress in the interlayer causes the displacement of an elastomer point to scale with the Laplacian of the hydrostatic stress [6,8].

As illustrated by Dillard [6] for a general loading of a plate supported on an elastomeric foundation and by Lefebvre et al. [7] for a double cantilever beam (DCB) specimen containing an elastomeric interlayer, and extended by Ghatak et al. [8] for the variation of the peel stress in the peeling direction, stresses in the elastomeric foundation significantly deviate from that predicted by the Winkler solution due to the constraint of incompressibility. For incompressible elastomers, the governing differential equation becomes sixth order (rather than the conventional uncoupled fourth order for Winkler foundations) that results in exaggerated oscillations in displacements and peel stresses.

Ghatak et al. [8] employed an LEFM approach to correlate the reaction force and the debond length to the fracture energy of the interface and the geometric and material parameters. Their analysis yielded a much slower decay of the oscillatory peel stress characterized by the length scale $(D_p h^3/E)^{1/6}$ as opposed to $(D_p h/E)^{1/4}$ predicted by the Winkler solution and resulted in the scaling of the pull-off force as $P_c \sim (D_p/E)^{1/3}\sqrt{\mathcal{G}_c E/h}$. The LEFM approach uses the fracture energy, $\mathcal{G}_c$, as the measure of the adhesion integrity. This represents the energy required for an existing debond to grow by a unit area and tacitly treats the debond tip as a mathematical point. This approach usually breaks down in large-scale bridging problems [9] in which there is a finite-size zone holding tractions in the wake of the debond, as seen, for example, during fibrillation of pressure-sensitive adhesives (PSA) or in fiber bridging in composites.

An approach suitable for large-scale bridging problems [9] is using the cohesive zone model (CZM). It employs a traction-separation (TS) relation to phenomenologically model debonding when two adjoining surfaces are separated. This allows debonding to nucleate and propagate when the interface is stressed and the appropriate criteria are satisfied. The often used TS relations [10–12] involve two significant parameters: the fracture energy,

[1]Present address: Dow Chemical Company, Freeport, TX 77541.
[2]Corresponding author.

Contributed by the Applied Mechanics Division of ASME for publication in the Journal of Applied Mechanics. Manuscript received October 7, 2016; final manuscript received October 10, 2016; published online November 7, 2016. Assoc. Editor: Kyung-Suk Kim.

$\mathcal{G}_c$, and the interfacial strength, T_c, to characterize the interfacial interaction, though other metrics are sometimes explicitly given. By using these two parameters, the CZM approach bridges the gap between a strength-based criterion and the fracture energy-based LEFM approach to model failure/debonding. For cohesive cracking in a medium of Young's modulus E^* and characteristic length l, Bao and Suo [9] pointed out that in the CZM approach the nondimensional group $T_c^2 l/\mathcal{G}_c E^*$ governs the transition from large-scale bridging (large process zone, strength driven, LEFM not valid) to small-scale bridging conditions (small process zone, fracture energy driven, LEFM applicable).

Tang and Hui [13] analyzed the debonding of a rigid cylindrical punch of radius a from an elastic interlayer of Young's modulus E using a Dugdale-type TS relation and showed that the single nondimensional number $\chi = (T_c^2 a/E\mathcal{G}_c)g(a/h)$ dictates the size of the process zone (CZ) where $\mathcal{G}$ is a function of a/h. With CZ size monotonically decreasing with χ, the global response transitions from a strength (T_c) dominated regime to an energy ($\mathcal{G}_c$) dominated regime. The pull-off force scales as $\sqrt{\mathcal{G}_c E/a}\sqrt{1/g(a/h)}$ in the energy dominated region ($\chi \gg 1$), and equals $\pi a^2 T_c$ in the strength dominated region.

The CZM has been widely applied to analyze splitting of two adherends [14–20] in a double cantilever beam (DCB) configuration. In these investigations, the effective interaction between two adherends is modeled by smeared traction-separation relations without separate consideration of the compliance of the adhesive layer and the interfacial debonding between the adhesive and the adherend. Therefore, it is not obvious how the modulus and the thickness of the adhesive layer, the interfacial adhesion, and the deformability of the adherends affect the mechanics of adhesive/interfacial debonding. Some investigators [3,5] included the effect of the adhesive compliance by setting the Winkler foundation stiffness equal to the modulus to thickness ratio of the adhesive. However, a Winkler foundation approach, as discussed earlier, is unsuitable when analyzing peeling from an elastomeric layer [6,8].

With the goal of simulating interfacial damage/debonding during displacement-controlled peeling of an overhanging plate from an elastomeric layer bonded to a rigid base, a TS relation is considered here for the elastomer/plate interface. We use a semi-analytical method to find the evolution of damage and debonding as vertical displacement is gradually increased at the edge of the overhang. The approximate formulation is built on earlier works of Dillard [6] and Ghatak et al. [8] for modeling the elastomeric foundation. The key contribution of this work is the consideration of the CZM at the plate/interlayer interface.

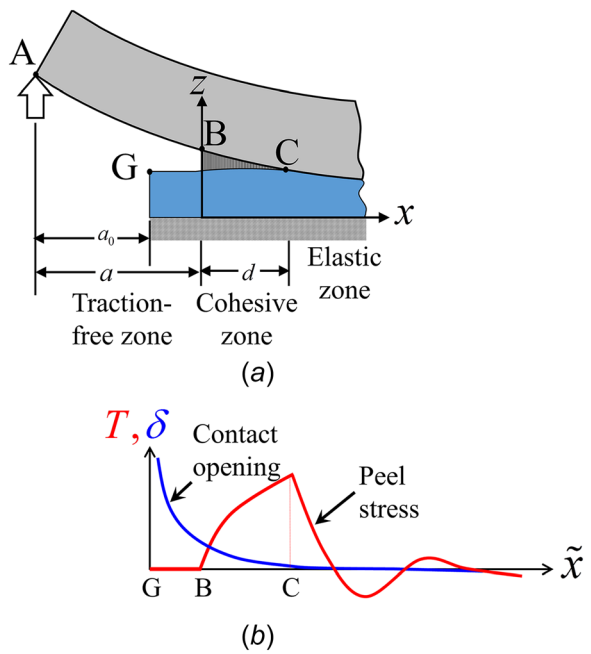

Fig. 1 Sketch of (*a*) the problem studied, and (*b*) various zones near the debond tip B after it has moved in the $\tilde{x}$ direction by the distance $a-a_0$. Also, schematically plotted are variations of the peel stress (normal traction) and the corresponding contact opening (displacement jump) along the $\tilde{x}$ -axis. (Color is available in the online version).

Problem Description and Analysis

The problem exhibited in Fig. 1(*a*) consists of a flexible plate adhered to an elastomer layer (interlayer) that is firmly bonded to a stationary rigid base so that debonding can occur only at the plate/elastomer interface when a monotonically increasing vertical displacement δ_A is applied at point A of the plate edge. This configuration is the same as the asymmetric wedge test configuration used by Ghatak et al. [8] and is often referred to as a small angle peel test [21]. Plane strain bending deformations of the system are described and analyzed by using a rectangular Cartesian coordinate system, xyz, with origin at the moving debond tip as shown in Fig. 1(*a*). The origin of the fixed rectangular Cartesian coordinate system $\tilde{x}yz$ is at the corner point G depicted in Fig. 1(*a*). It is tacitly assumed that the system extends to infinity in the y-direction and deformations of the plate and the elastomer layer in the xz -plane are analyzed.

Deformations of the Plate. Plane strain deformations of the thin flexible plate are assumed to be governed by the Kirchhoff–Love plate theory [22] for infinitesimal deformations with the y-displacements set equal to zero. Bending is assumed to be the dominant deformation mode of the plate[3].

$$\Lambda^4 w_p = -T/D_p \tag{1}$$

Here, $\Lambda^n = d^n/dx^n$, and w_p is the vertical displacement of a point in the plate, T is the normal traction acting on the plate, and $D_p = E_p t^3/12(1-\nu_p^2)$ is the plate flexural rigidity in terms of its thickness t, Young's modulus E_p, and Poisson's ratio ν_p.

Plate/Elastomer Interface. Following previous works [13,24], we assume that damage/debonding is triggered only by the peel stress at the plate/elastomer interface, i.e., the interface is much stronger in the axial than in the normal direction. For equally weak adhesion in both directions at the two interfaces, one interface will have a shearing/peeling bias dictated by the asymmetry due to the adherend stiffness mismatch. Therefore, even with our simplifying assumption, global results such as the strength or the effective interaction between the flexible plate and the rigid base would depend upon this asymmetry. This is not analyzed in the present work.

The interaction is assumed to be characterized by a bilinear TS relation depicted in Fig. 2 and described by Eq. (2).

$$T = \begin{cases} K_e\delta & (0 \le \delta \le \delta_c) \\ K_s(\delta_f - \delta) & (\delta_c \le \delta \le \delta_f) \\ 0 & (\delta_f \le \delta) \end{cases} \tag{2}$$

Here, K_e is the slope of the portion OM of the TS curve and $K_s = T_c/(\delta_f - \delta_c)$, where T_c is the maximum normal traction supported by the interface. The point M (δ_c, T_c) signifies the initiation of damage (softening) and the point N $(\delta_f, 0)$ the onset of debonding. The energy release rate at the initiation of debonding equals area of the triangle OMN, i.e.,

[3]The classical short beam effect dictated by the ratio a_0/t may affect the compliance of the beam due to shear deformations of the flexible adherend. The minimum value of a_0/t used for demonstrating the model predictions is 2, which is expected to underestimate the plate compliance by 25% [23].

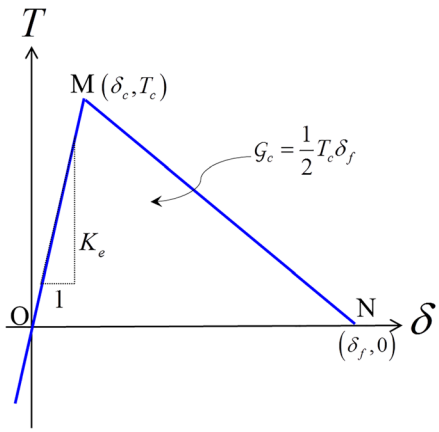

Fig. 2 A bilinear TS relation

$$\mathcal{G}_c = T_c\delta_f/2 \tag{3}$$

The initial slope K_e in Eq. (2) is assigned a large enough value to not influence the debond initiation and propagation at the plate/elastomer layer interface. For the present problem, we also assume that it satisfies the inequality given after Eq. (18). Because of monotonically increasing displacement δ_A applied at point A, no unloading at any point of the interface is expected to occur prior to the initiation of debonding there.

It is anticipated that a CZ will develop near the corner G in Fig. 1(*a*) followed by debonding there. The subsequent propagation of the debond with a CZ at its front and the associated distribution of the interfacial peel stress and the separation at the interface are schematically illustrated in Fig. 1(*b*).

Deformations of the Elastomeric Layer. Plane strain deformations of the homogeneous, incompressible, isotropic, and linearly elastic elastomer layer with the body and the inertia forces neglected are governed by

$$p_x = \mu(u_{xx} + u_{zz}), p_z = \mu(w_{xx} + w_{zz}) \tag{4}$$

$$u_x + w_z = 0 \tag{5}$$

where p is the hydrostatic pressure not determined by the deformations, μ (= $E/3$, where E is Young's modulus) is the shear modulus, u and w are the displacement components in the x- and the z-directions, respectively, $p_x = (\partial p/\partial x)$, and Eq. (5) expresses the incompressibility constraint. The following boundary conditions for the elastomer layer are presumed:

$$u(x,0) = w(x,0) = 0; u(x,h) = 0 \text{ for } x \geq 0 \tag{6}$$

$$-p(x,h) + \mu\frac{\partial w}{\partial z}(x,h) = 0 \text{ for } -(a-a_0) \leq x < 0$$

That is, the elastomer particles are firmly bonded to the stationary rigid base, there is no slip at the elastomer/plate interface, and horizontal displacements of the plate particles are negligible, and the debonded surface of the elastomeric layer has null traction. The additional boundary condition for the upper surface $z = h, x > 0$ of the interlayer as well as those on the free surface $\tilde{x} = 0$ will be stated below.

It should be noted that the problem studied here is not equivalent to a DCB problem with an adhesive layer of thickness $2h$ since the horizontal displacements of the interlayer particles on the surface $z = 0$ are set equal to zero.

Approximate Solution of the Governing Equations. Using assumptions analogous to those made in the classical lubrication theory [25] for thin films, i.e., $|u_{zz}| \gg |u_{xx}|$, and $p_z = 0$, Eq. (4) simplifies to

$$p_x = \mu u_{zz}, \quad p_z = 0 \tag{7}$$

When employing the lubrication theory, deformations cannot be accurately predicted over a length of order h from the left edge [25]. Nevertheless, we use these assumptions for simplicity. In the approximate solution sought here, the boundary condition of null traction on the left edge $\tilde{x} = 0$ is not satisfied. Similar assumptions were used by Ghatak et al. [8] in their LEFM analysis of this problem.

Integrating Eqs. (5) and (7) and using boundary conditions (6) gives

$$u(x,z) = \frac{1}{2\mu}\frac{dp}{dx}(z^2 - hz), w(x,z) = -\frac{1}{2\mu}\frac{d^2p}{dx^2}\left(\frac{z^3}{3} - h\frac{z^2}{2}\right) \tag{8}$$

The vertical displacement, w_f, of points on the elastomer top surface is given by

$$w(x,h) = w_f(x) = \frac{h^3}{12\mu}\frac{d^2p}{dx^2} \tag{9}$$

The normal stress, $\sigma_{zz}(x,z) = -p(x) + \mu\partial w/\partial z$, at the elastomer top surface becomes $\sigma_{zz}(x,h) = -p(x)$. The continuity of normal traction across the elastomer/plate interface implies that $p = -T(\delta)$ where

$$\delta = w_p - w_f \tag{10}$$

is the separation/opening at an interfacial point. Substitution for w_p from Eq. (10) and for w_f from Eq. (9) into Eq. (1) results in the following sixth order ordinary differential equation (ODE) for T.

$$-\Lambda^6 T + \frac{12\mu}{h^3}\left(\Lambda^4\delta + \frac{1}{D_p}T\right) = 0 \tag{11}$$

Substitution for T in terms of δ from Eq. (2) into Eq. (11) gives a sixth order ODE in δ, which is solved under the pertinent boundary conditions. In principle, any TS relation can be used and the resulting nonlinear ODE can be numerically solved using, for example, a shooting method.

Corresponding to the three relations in Eq. (2) that hold, respectively, in the free/debonded zone $(-a \leq x \leq 0, \delta \geq \delta_f)$, the CZ $(0 \leq x \leq d, \delta_c \leq \delta < \delta_f)$ and the bonded zone $(d \leq x < \infty, \delta \leq \delta_c)$, three ODEs from Eq. (11) are deduced; these zones are shown in Fig. 1(*b*). The variables are nondimensionalized (normalized) as $X = x\beta$, and $\Delta = \delta/\delta_f$ where $\beta = (12\mu/D_p h^3)^{1/6}$, i.e., we have used different length scales to normalize the x-axis and the transverse opening displacement, δ. The nondimensional debond length, a ($A = a\beta$), and the CZ size, d ($D = d\beta$), are denoted by A and D, respectively. The three ODEs and their solutions are listed below.

Debonded/free region $(-A \leq X \leq 0)$: Since $T = 0$, Eq. (11) becomes

$$\Lambda^4\Delta = 0 \tag{12}$$

where $\Lambda = d/dX$. The solution of Eq. (12) is

$$\Delta(X) = D_1X^3 + D_2X^2 + D_3X + D_4 \tag{13}$$

where $D_1, ..., D_4$ are integration constants. The same notation with different numeric subscripts will be used below for other integration constants.

Cohesive zone $(0 \leq X \leq D)$: Now Eq. $(2)_2$ holds, and Eq. (11) reduces to

$$(\Lambda^6 + \eta_s^2\Lambda^4 - 1)\Delta + 1 = 0 \tag{14}$$

where $\eta_s = (12\mu/K_s h^3)^{1/2}\beta^{-1}$. The solution of Eq. (14) depends on the roots of the characteristic cubic equation, $(\Lambda^2)^3 + \eta_s^2(\Lambda^2)^2 - 1 = 0$. The three roots for Λ^2 are real and distinct if $\eta_s > \eta_s^c (= (27/4)^{1/6})$; they are real and at least two are

equal if $\eta_s = \eta_s^c$, and one root is real and the other two are complex conjugates otherwise. Listed below are the general solutions of Eq. (14) for these three cases:

Case I: $\eta_s < \eta_s^c$

$$\Delta(X) = D_5 e^{-pX} + D_6 e^{pX} + e^{-qX}(D_7 \cos(qX) + D_8 \sin(qX)) + e^{qX}(D_9 \cos(rX) + D_{10} \sin(rX)) + 1 \tag{15}$$

Case II: $\eta_s = \eta_s^c$

$$\Delta(X) = D_5 e^{-pX} + D_6 e^{pX} + (D_7 \cos(qX) + D_8 \sin(qX)) + X(D_9 \cos(rX) + D_{10} \sin(rX)) + 1 \tag{16}$$

Case III: $\eta_s > \eta_s^c$

$$\Delta(X) = D_5 e^{-pX} + D_6 e^{pX} + (D_7 \cos(qX) + D_8 \sin(qX)) + (D_9 \cos(rX) + D_{10} \sin(rX)) + 1 \tag{17}$$

Here p, q, and r are found from roots of the characteristic cubic equation. Note that constants $D_5, \ldots, D_{10}$ appearing in Eqs. (15)–(17) may have different values.

Bonded/Elastic zone ($D \le X \le \infty$): Using Eq. $(2)_1$, Eq. (11) becomes

$$(\Lambda^6 - {\eta_e}^2 \Lambda^4 - 1)\Delta = 0 \tag{18}$$

where $\eta_e = (12\mu/K_e h^3)^{1/2}\beta^{-1}$. For ${\eta_e}^2 \ll 1$, and assuming that $\Lambda^4\Delta$ is finite, Eq. (18) reduces to the ODE, $(\Lambda^6 - 1)\Delta = 0$, which was analyzed in Refs. [6] and [8] that considered perfect bonding at the interface. Note that ${\eta_e}^2 \ll 1$ can be satisfied by assigning a very large value to K_e. The general solution of Eq. (18) for ${\eta_e}^2 \ll 1$ is

$$\Delta(X) = D_{11} e^{-X} + D_{12} e^{X} + e^{-\frac{X}{2}}\left(D_{13} \cos\left(\frac{\sqrt{3}}{2}X\right) + D_{14} \sin\left(\frac{\sqrt{3}}{2}X\right)\right) + e^{\frac{X}{2}}\left(D_{15} \cos\left(\frac{\sqrt{3}}{2}X\right) + D_{16} \sin\left(\frac{\sqrt{3}}{2}X\right)\right) \tag{19}$$

A noteworthy feature of the governing Eqs. (14) and (18) is that it has both sixth order and fourth order derivatives. The former arises due to deformations of the elastomeric layer and the latter due to the interfacial normal tractions exerted on the plate by the interface acting as a Winkler foundation.

Boundary conditions for evaluating constants in Eqs. (13)–(19). The 16 integration constants appearing in Eqs. (13)–(19), the size D of the CZ, and either the separation Δ_B at point B prior to the initiation of debonding or the length A during propagation of the debonded region are determined from the following 18 conditions.

The bending moment vanishes at the left end where the vertical displacement is prescribed. Thus,

$$\Delta(-A) = \Delta_A, \Delta''(-A) = 0 \tag{20}$$

Here and below, we have used the notation $\Delta' = d\Delta/dX$. The continuity of the plate deflection (w_p), the slope (w_p'), the bending moment ($\sim w_p''$), the shear force ($\sim w_p'''$), and the normal traction ($\sim w_p''''$) at points B and C shown in Fig. 1(*b*) gives the following ten conditions at these points where superscripts + and − denote, respectively, the locations just on the right and just on the left side of a point.

At point B :

$$\Delta(0^-) = \Delta(0^+) + \eta_s^{-2}\Delta''(0^+), \Delta'(0^-) = \Delta'(0^+) + \eta_s^{-2}\Delta'''(0^+), \Delta''(0^-) = \Delta''(0^+) + \eta_s^{-2}\Delta''''(0^+),$$
$$\Delta'''(0^-) = \Delta'''(0^+) + \eta_s^{-2}\Delta'''''(0^+), \Delta''''(0^-) = \Delta''''(0^+) + \eta_s^{-2}\Delta'''''(0^+) \tag{21}$$

At point C:

$$\Delta(D^-) + \eta_s^{-2}\Delta''(D^-) = \Delta(D^+) - {\eta_e}^{-2}\Delta''(D^+), \Delta'(D^-) + \eta_s^{-2}\Delta'''(D^-) = \Delta'(D^+) - {\eta_e}^{-2}\Delta'''(D^+),$$
$$\Delta''(D^-) + \eta_s^{-2}\Delta''''(D^-) = \Delta''(D^+) - {\eta_e}^{-2}\Delta''''(D^+), \Delta'''(D^-) + \eta_s^{-2}\Delta'''''(D^-) = \Delta'''(D^+) - {\eta_e}^{-2}\Delta'''''(D^+)$$
$$\Delta''''(D^-) + \eta_s^{-2}\Delta'''''(D^-) = \Delta''''(D^+) - {\eta_e}^{-2}\Delta'''''(D^+) \tag{22}$$

The relative vertical displacements at these points can be written as

$$\Delta(0^-) = \Delta_B \text{ and } \Delta(D^+) = \Delta_c \tag{23}$$

with $\Delta_B = 1$ after debonding initiates at point G. Until then, Δ_B is treated as a variable with length A of the traction-free portion known. The nondimensional contact opening Δ_c at point C equals T_c/K_e.

The assumption of zero relative separation at points far away from point C can be stated as

$$\lim_{X\to\infty} \Delta = 0 \tag{24}$$

Finally, the overall equilibrium requires that the reaction (or the shear) force, p_A, at point A, equal the total restoring force exerted by the elastomeric interlayer on the flexible plate. From the Kirchhoff–Love plate theory, one gets $p_A = Dw_p'''(-a) = D_p\beta^3\delta_f\Delta'''(-A)$. It equals the peel stress integrated over the interface, i.e., $\beta^{-1}\int_0^\infty T(\delta)dX$. Thus

$$\frac{1}{D_p\beta^4\delta_f}\int_0^\infty T(\delta)dX = \Delta'''(-A) \tag{25}$$

The decay condition (24) implies that constants D_{12}, D_{15}, D_{16} must be zero. Equation (20) gives Eq. (26) upon eliminating D_2, and Eq. (1) is used to reduce Eqs. (25) to (27).

$$2D_1A^3 - D_3A + \Delta_B - \Delta_A = 0 \tag{26}$$

$$\eta_s^{-2}D - \eta_s^{-2}\int_0^D \Delta dX + {\eta_e}^{-2}\int_D^\infty \Delta dX - 6D_1 = 0 \tag{27}$$

Constants $D_1,\ldots, D_{14}$ are found in terms of A and D by simultaneously solving algebraic equations resulting from conditions (21)–(23) using the software MATHEMATICA [26]. Equation (27) is simplified by substituting for Δ from Eqs. (15)–(17) and (19). By using the function FINDROOT, the transcendental Eqs. (26) and (27) are then numerically solved for Δ_B and D until $\Delta_B = 1$, i.e., for the initiation phase, and for A and D for the propagation phase.

Results and Discussion

Prior to discussing the results, we note that the problem has the following independent parameters:

$$\text{elastomer}: h, \mu, \nu$$
$$\text{plate}: E_p, \nu_p, t$$
$$\text{interface}: \mathcal{G}_c, \delta_f = 2\mathcal{G}_c/T_c, K_e$$
$$\text{initial free region}: a_0$$
$$\text{loading}: \delta_A$$

Because of assuming the interlayer to be perfectly incompressible, i.e., $\nu = 0.5$, we have ten independent variables. By using μ and h to nondimensionalize the remaining variables, we get the following eight nondimensional parameters that govern the behavior of the system:

$$\alpha, \phi, \Delta_A, T_c/\mu, K_e h/E, A_0, a_0/t, \nu_p$$

where $\alpha = (D_p/\mu h^3)^{1/3}$, $A_0 = a_0\beta$, $\phi = T_c^2 h/E\mathcal{G}_c$, and $\beta^{-1} = (12\mu/D_p h^3)^{-1/6}$. The length scale β^{-1} is related to the deformability of the interlayer [6,8] relative to that of the flexible plate, α represents the geometric confinement [27] and equals the ratio of the bending stiffness of the plate to that of the interlayer, and ϕ is an adhesion parameter that dictates the CZ size [9,27].

Because of using the approximations in our formulation, the CZ size (D) and the length (A) depend on Δ_A and the parameter $\eta_s = (12\mu/K_s h^3)^{1/2}\beta^{-1} \approx 3.238\sqrt{(\mathcal{G}_c\mu/T_c^2)(D_p/\mu h^6)^{1/3}} \approx 1.87\sqrt{\alpha/\phi}$ appearing in Eq. (14). Thus, α and ϕ govern the response through η_s. The effects of η_e appearing in Eq. (18) and Δ_c are assumed to be negligible since $\eta_e \ll \eta_s$ and $\Delta_C \ll \Delta_B$ when $K_e h/E \gg 1$. Here the effect of the following three variables on the solution has been studied.

$$\eta_s, \Delta_A, A_0$$

The values of parameters used in the numerical simulations are listed in Table 1.

Unless otherwise mentioned, the results are computed for $A_0 = 2$ and $\eta_s = 2$. Evolutions of the plate deflection, $W_p = w_p/\delta_f$, and the nondimensional peel stress, T/T_c, are plotted in Fig. 3 as functions of the global horizontal distance measured from point G shown in Fig. 1(*a*). The negative values of $\tilde{X} = \beta\tilde{x}$ correspond to points on the traction free overhanging portion of the plate. As expected for the bending of a plate on an elastomer foundation, the plate deflection exhibits decaying oscillatory distribution. The computed deflection profile agrees well with that reported by Ghatak et al. [8] and with that numerically computed using the finite element method (FEM) [27]. Plots of the spatial distribution of the peel stress exhibited in Fig. 3(*b*) reveal that with continued loading, a CZ develops and the peel stress reduces to zero at the initial debond tip, i.e., $\tilde{X} = 0$, at a critical value, $\Delta_{A0} = 3.1$, of the applied nondimensional displacement. The comparison of the predicted peel stress distributions with the solution of Ghatak

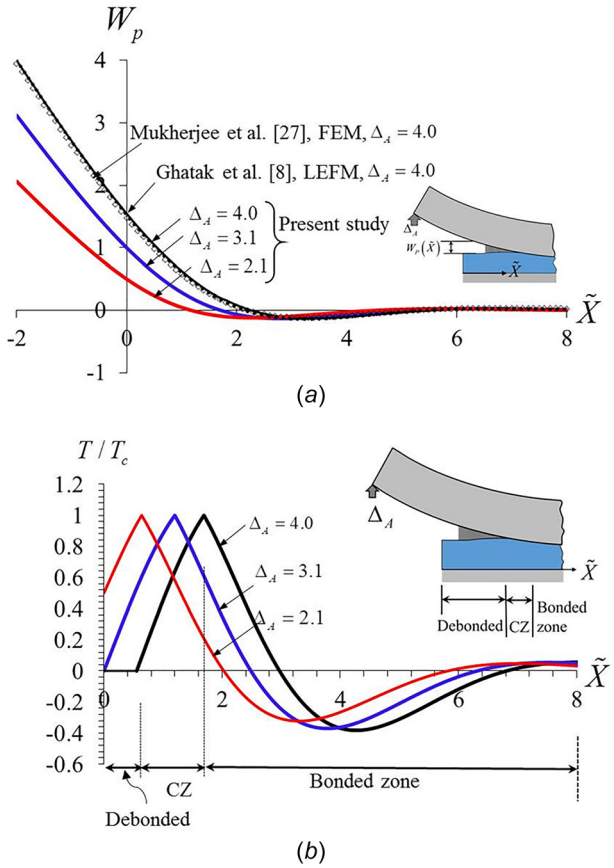

Fig. 3 For three values of the nondimensional applied displacement, Δ_A, distributions of the nondimensional (*a*) plate deflection and (*b*) peel stress (T/T_c) on the global horizontal axis $\tilde{X} = \beta\tilde{x}$. For $\Delta_A = 4.0$, the three regions around a debond are marked in (*b*).

Table 1 List of values of parameters used in the FE simulations used for comparison exhibited in Fig. 4.

	Plate				Elastomer		Interface		
Dimensionless parameters	a_0 (mm)	t (mm)	E_p (MPa)	ν_p	E (MPa)	h (μm)	T_c (MPa)	$\mathcal{G}_c$ (N/m)	K_e (N/mm^3)
$A_0 = 2$ $\eta_s = 2$ $\Delta_A = 4$	2	1	1201.5	0.3	15	817	0.04	0.029	10^6
$A_0 = 2$ $\eta_s = 1.5$ $\Delta_A = 4$	2				6.33	873.4			
$A_0 = 3$ $\eta_s = 2.25$ $\Delta_A = 4$	2.83				21.36	817			

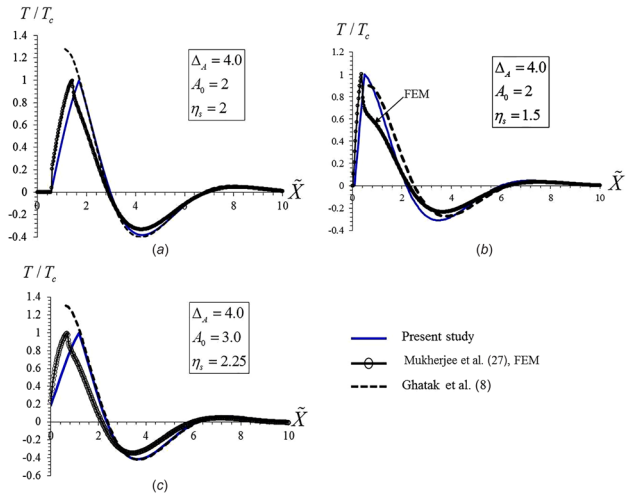

Fig. 4 Comparisons of predicted peel stresses from present work with those predicted by the LEFM [8] solution and computed using the FEM [27]. The nondimensional input parameters are listed in the insets.

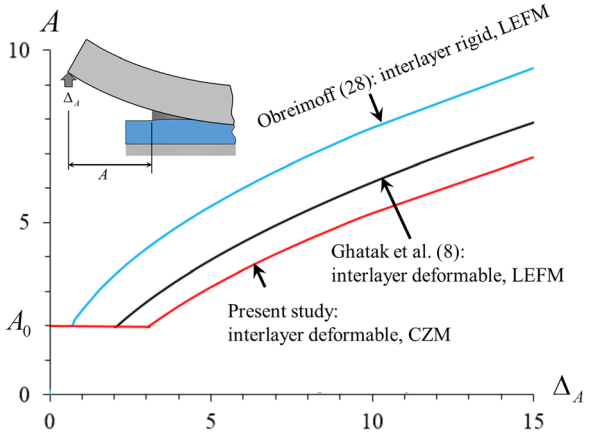

Fig. 5 Nondimensional traction-free length as a function of the applied nondimensional displacement

et al. [8] is exhibited in Fig. 4(*a*) for the propagating debond at $\Delta_A = 4.0$. Whereas the debond tip in their work is the point where the peel stress is the maximum, it is the point of zero peel stress in our analysis. The point with the maximum peel stress, $T/T_c = 1$, in the present work is the tip of the CZ, with the value of T_c regarded as an intrinsic property of the pair of interacting materials. The presently predicted peel stress distribution at $\Delta_A = 4.0$ agrees reasonably well with that computed using the FEM [27] with the FEM predicting 0.6% smaller traction-free length A and 24% smaller CZ length D than that given by the current approximate analysis. These differences are possibly due to using the lubrication theory, neglecting shearing deformations of the plate and other approximations made in the present work. For example, deformations computed with the FEM reveal that at $\Delta_A = 4.0$, the values of u_{xx} and u_{zz} at the point ($x =$ location of predicted damage tip,$z = h/2$) are -0.00069 and -0.00096, respectively. Thus, the lubrication theory approximation, $|u_{xx}| \ll |u_{zz}|$, is inappropriate. However, as shown below, the presently computed pull-off force agrees well with that found from the solution of the plane strain problem equations using the FEM over a broad range of values of η_s. As suggested by an anonymous reviewer, we compare in Figs. 4(*b*) and 4(*c*) our results with those computed using the FEM and Ghatak et al.'s [8] solution for $\eta_s = 1.5$ and 2.25. While our analysis captures the oscillatory feature of the peel stress distributions, the CZ size is overestimated. As mentioned previously, this may be partly due to neglecting the shear deformations of the plate.

The computed dimensionless length A as a function of the applied displacement Δ_A and predictions of the LEFM analysis with [8] and without [28] the interlayer deformability accounted for are exhibited in Fig. 5. For a deformable interlayer, the length A can be found from[4]

$$\Delta_A^2 = \frac{\eta_s^{-2} A^4}{9\Omega(A)} \quad \text{where}$$

$$\Omega(A) = \frac{8A^4(12 + 46A + 72A^2 + 56A^3 + 21A^4 + 3A^5)}{3(6 + 12A + 9A^2 + 2A^3)^3} \tag{28}$$

[4]Equation (28) has been reported to have been derived from the energy minimization approach [8]. However, starting from the load-displacement relation derived in their approach and using $-\frac{\partial}{\partial A}\left(\int_0^{\Delta_A} P_A d\Delta_A\right) = \eta_s^2/2$, one obtains $\Omega(A) = 4A^4(2 + 3A + A^2)/(6 + 12A + 9A^2 + 2A^3)^2$ that slightly differs from that given in Eq. (28).

In the limit of a relatively rigid interlayer or a very pliable plate ($A \gg 1$), Eq. (28) reduces to Obreimoff's [28] result $\Delta_A^2 = \eta_s^{-2} A^4/9$ in terms of the current nondimensional variables. As can be observed from Fig. 5, the debond length at a given applied edge displacement is overpredicted if the deformability of the interlayer is neglected. Our results predict even smaller debond length at a given applied edge displacement due to the consideration of the CZ at the debond tip (B) and a constant peak stress at the damage tip (C).

Evolutions of the CZ size, the opening at the debond tip, and the slope of the plate at the debond tip as functions of the applied edge displacement are exhibited in Fig. 6. The dashed lines in these plots correspond to the damage growth at the corner point G until debonding occurs there and the solid lines with the subsequent propagation phase. Each dashed line intersects the corresponding solid one when $\Delta_B = 1$ at point G. One can observe that the CZ size increases with the applied edge displacement until debonding ensues at point B. During the propagation phase, the CZ size slowly decreases. This trend was also noted in Refs. [19] and [20] for softening interactions involved in a DCB geometry and in the context of cohesive cracking [29]. The slow decrease in the CZ size during propagation agrees with the observation that the slope at the debond tip (B) increases while the plate deflection stays constant.

The maximum CZ size (D_0) at the onset of debonding is plotted in Fig. 7(*a*) as a function of η_s for three values of the initial overhang length, A_0, and as a function of A_0 for two values of η_s. One can see that D_0 increases (decreases) with an increase in η_s (A_0),

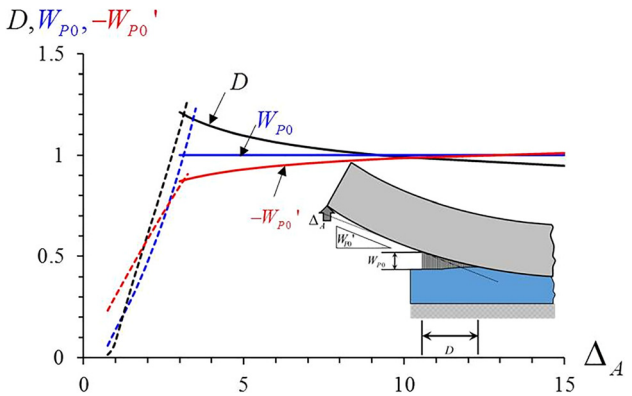

Fig. 6 Nondimensional CZ size, the plate deflection at the debond tip, and the plate slope at the debond tip versus the nondimensional applied displacement. The dashed lines represent results prior to the initiation of debonding.

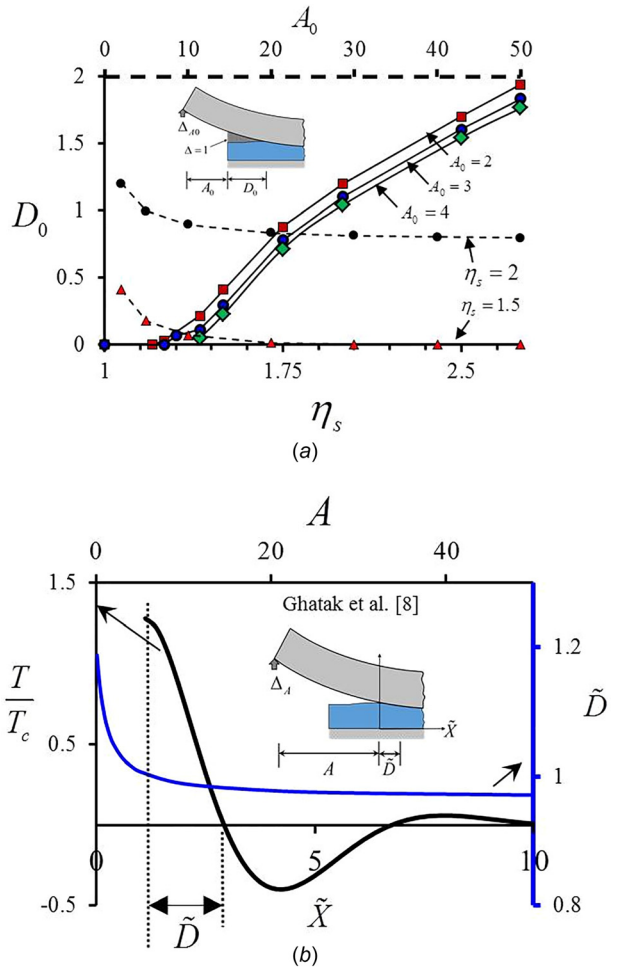

Fig. 7 (*a*) The CZ size at debond initiation versus η_s for three values of the initial overhang length A_0 (solid lines) and versus A_0 for two values of η_s (dashed lines) and (*b*) peel stress distribution at $\Delta_A = 4.0$ and the size of the tensile region near the debond tip as a function of the debond length given by Ghatak et al.'s [8] solution

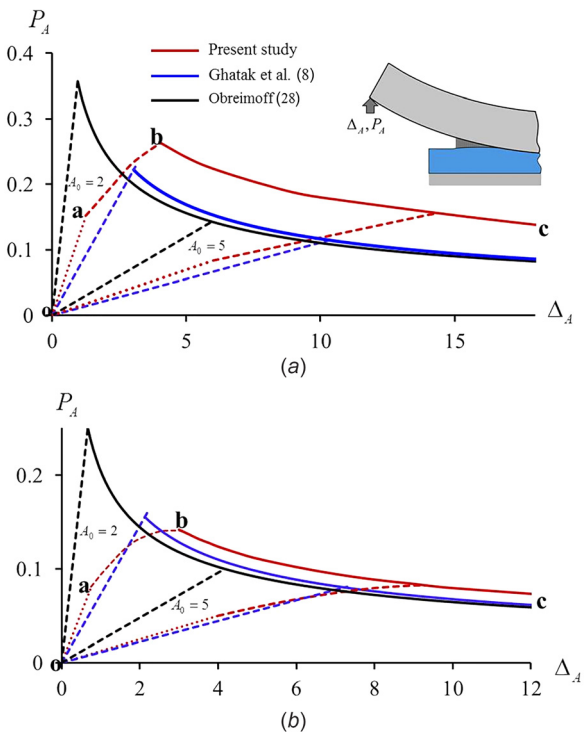

Fig. 8 Nondimensional load versus the applied nondimensional displacement for (*a*) $\eta_s = 1.4$ and (*b*) $\eta_s = 2$. The dotted line (*oa*) and the dashed line (*ab*) represent results, respectively, prior to the initiation of damage and between damage initiation and debonding initiation. The solids portion (*bc*) are for debond propagation.

although dependence on A_0 is much weaker than that on η_s. Recalling that $\eta_s \sim \sqrt{(\mathcal{G}_c\mu/T_c^2)(D_p/\mu h^6)^{1/3}}$, the former is attributed to an increase in the cohesive length $\mathcal{G}_c\mu/T_c^2$ relative to the length $(D_p/\mu h^6)^{1/3}$ arising from the material and the system geometry. An interesting finding regarding the dependence of the CZ size on η_s is that the CZ size becomes vanishingly small at $\eta_s <\sim 1.3$. Arguing that the length of the CZ phenomenologically represents the fingering zone [30,31] observed in peeling experiments, the aforementioned finding is reminiscent of the reported observation [31,32] that the fingerlike zones are physically discernible only beyond a finite value of the geometric confinement parameter $(D_p/\mu h^3)^{1/3}$. The slow decrease of the CZ size with the debond length is similar to the dependence of the near-tip tensile zone size $(\tilde{D})$ on the length (A) predicted by Ghatak et al.'s [8] LEFM analysis and exhibited in Fig. 7(*b*).

The dimensionless load–displacement (LD) relation from Ghatak et al.'s [8] analysis is given by $P_A = 6\Delta_A/(6 + 12A + 9A^2 + 2A^3)$, which for a rigid interlayer reduces to $P_A = 3\Delta_A/A^3$. The LD curves predicted in the present study are plotted and compared with the LEFM results in Fig. 8 for two values of $\eta_s = 2$ and 1.4, and for two initial overhang lengths $A_0 = 2$ and 5. In these plots, the dotted and the dashed portions are used to represent results prior to debonding initiation, and the solid lines are for the subsequent propagation phase. The dotted segment *o-a* (labeling included only in the $A_0 = 2$ plot) corresponds to the phase when the peel stress at the corner B traces the segment OM of the TS relation. It is shown in Appendix that the LD relation for the portion *o-a* satisfies $P_A = 6\Delta_A/(3A + 6A^2 + 2A^3)$. The dashed segment *a-b* corresponds to the formation of the CZ near corner G and the peel stress at the corner tracing the portion MN of the TS relation. This causes the kink observed in the initial rising part *o-a-b* of the LD curve. The segment *b-c* corresponds to the propagation phase in which the load decreases with increasing displacement in a similar fashion ($P_A \propto {\Delta_A}^{-1/2}$) as that in the LEFM results. The offset of the curve *b-c* from the LEFM curves is attributed to the additional compliance induced by the interfacial softening effect resulting in a smaller debond length at a given applied displacement (recall Fig. 5). The offset is found to be larger at $\eta_s = 1.4$ despite the CZ size being much smaller than that at $\eta_s = 2$. This seems to contradict at first sight the expectation that the results will converge to the LEFM results for vanishing CZ sizes. In order to understand the reasons for this difference, we revisit Ghatak et al.'s [8] solution (see Appendix) to find the expected solution for vanishingly small CZ size. In order to limit the damage/debond tip peel stress to T_c, we modify their debond tip boundary condition to $W''''(0+) = -\eta_s^2$. This gives the following relation between the load, the applied edge displacement, and the length A: $P_A = (3\Delta_A/(9+12A+6A^2+A^3)) + (1/\eta_s^2)(3(2+A)/(9+12A+6A^2+A^3))$. For very long traction-free lengths, $A \gg 1$, we get $P_A = (3\Delta_A/A^3) + (|3/A^2\eta_s^2|)$. The second term accounts for the debond tip peel stress tracing the path MN of the TS relation over a vanishingly small length near the debond tip and causes the aforementioned offset in the LD curve. One notes that the offset term will be negligible for sufficiently large values A dictated by the value of η_s.

The maximum values of P_A (pull-off force) are plotted on a log–log scale in Fig. 9 as a function of η_s for $A_0 = 2.83$ and

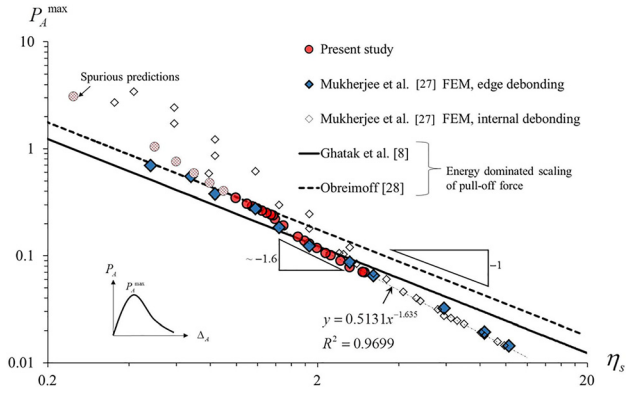

Fig. 9 For $A_0 = 2.83$, the peak load (pull-off force) as a function of the nondimensional number η_s on a log–log scale

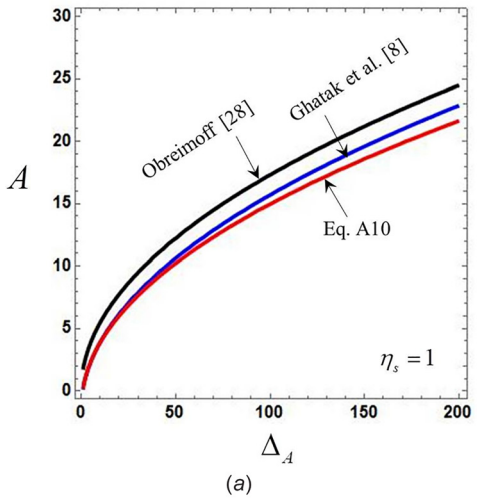

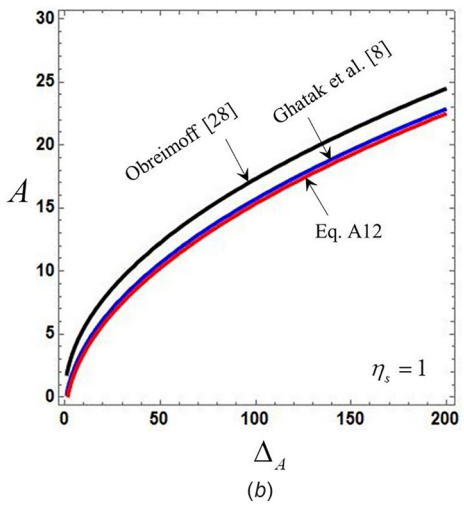

Fig. 10 The dimensionless debond length as a function of Δ_A from (*a*) Eq. (A10) and (*b*) Eq. (A12). Corresponding LEFM plots are included for comparison.

compared with those from the numerical solution of the plane strain problem using the FEM [27] for edge debonding mechanism. One can observe that the predicted pull-off force values decrease with an increase in η_s relatively faster for $\eta_s > 1.3$, while for smaller values of η_s, they follow a scaling similar to that of the LEFM predictions. The FEM predictions for edge debonding mechanisms also exhibit a similar trend, providing further credence to the present work. A power-law fit to the data points for $\eta_s > 1.3$ reveals the approximate scaling of the dimensionless pull-off force, ${P_A}^{max} \propto {\eta_s}^{-1.6}$ or in dimensional units, ${p_A}^{max} \sim D_p^{\frac{7}{30}} \mu^{-\frac{1}{30}} h^{\frac{1}{10}} \mathcal{G}_c^{\frac{1}{5}} T_c^{\frac{3}{5}}$ (exponents are approximate). Thus, the pull-off force is dominated by the cohesive strength, T_c, and weakly depends on the fracture energy $\mathcal{G}_c$ and other parameters. On the contrary, the LEFM results [8] give ${p_A}^{max} \sim D_p^{\frac{1}{3}} \mu^{\frac{1}{6}} h^{-\frac{1}{2}} \mathcal{G}_c^{\frac{1}{2}}$ (exponents are exact). That is, the pull-off force at sufficiently small values of $\eta_s (<\sim 1.3)$ does not depend on the cohesive strength and is dominated by the fracture energy. This knowledge can potentially be used to extract fracture energy values from the pull-off force data for a very thick elastomer layer, and the interface strength for a thin elastomer layer. The variation of the pull-off force with η_s agrees with the corresponding variation of the CZ size suggesting a transition from small-scale to large-scale bridging conditions [9]. We note that for $\eta_s < 1$, the present pull-off force predictions begin to deviate (the indicated data points with a different marker) from the expected LEFM scaling although the FEM predictions of edge debonding mechanism still satisfy the LEFM scaling. These way-off data points are due to errors introduced by the approximations made in the current work. However, as mentioned in the preceding paragraph, a longer initial overhang length will reduce this error and increase the range of η_s over which the pull-off force predictions are valid.

A major assumption made in this work is that debonding initiates only at the corner G. As reported in Refs. [27] and [34], debonding may initiate at interior points of the interface for elastomer interlayers for which the confinement quantified by $\alpha = (D_p/\mu)^{1/3}/h$ exceeds ~9. For $\alpha >\sim 9$, a CZ may begin to form over the interior of the interface at a distance $\sim \beta^{-1}$ from the edge; this is not captured by the present approach that considers the formation of only one CZ at the edge. Moreover, the opening at interior points may exhibit waviness when the parameter $\phi = T_c^2 h/\mathcal{G}_c E$ exceeds a critical value ≈ 5 [27]. The numerical solution of the plane strain problem using the FEM [27] gave values of α and ϕ when interfacial debonding will initiate from the edge and at interior points, and also of the pull-off force. Noting that $\eta_s \sim \sqrt{\alpha/\phi^{-1}}$, a number of computed values of the pull-off force for the strength dominated region in Fig. 9 corresponded to internal initiation rather than edge initiation for $\alpha > 9$. These are indicated using different markers in Fig. 9. It is encouraging to see that the present data points are on the same power-law fit as those from the numerical solution of the plane strain problem for $\eta_s >\sim 1$.

Conclusions

We have studied the initiation of damage and debonding at the corner of a flexible plate overhanging on and peeled from an elastomer layer firmly bonded to a rigid base. The analysis employs a bilinear traction–separation relation in a cohesive zone model (CZM) for the plate/elastomer interface, the lubrication theory for deformations of the elastomeric layer, and builds on the works of Dillard [6] and Ghatak et al. [8].

The key finding is that the single nondimensional number $\eta_s = 3.238\sqrt{(\mathcal{G}_c\mu/T_c^2)(D_p/\mu h^6)^{1/6}}$ governs the interfacial opening normalized by δ_f, the debond length and the CZ size normalized by $\beta^{-1} = (12\mu/D_p h^3)^{-1/6}$, and the load normalized by $D_p\beta^3\delta_f$. Here, T_c is the interfacial strength, $\mathcal{G}_c$ is the fracture energy of the interface, μ is the shear modulus of the elastomer, h is its thickness, D_p is the flexural rigidity of the plate, β^{-1} is the length scale of oscillations of the interfacial peel stress for bending of a Kirchhoff–Love plate on an elastomer foundation, and $\delta_f = 2\mathcal{G}_c/T_c$ is the debond tip opening. The CZ size decreases as η_s

decreases. Consequently, the response transitions from a strength dominated regime to an energy dominated regime. This is supported by numerical solutions of equations governing plane strain deformations of the system by the finite element method.

Besides its potential use as guiding design for load capacity, the scaling of the pull-off force could be utilized to extract values of T_c and $\mathcal{G}_c$ for the interface by suitably designing interlayer thickness and/or the flexural rigidity of the plate.

This approximate analysis is based on a number of restrictive assumptions and is certainly not rigorous enough to capture intricacies of the interfacial debonding of a confined elastomer layer. Nonetheless, the results provide insights to the adhesion community interested in soft matter adhesion.

Acknowledgment

The authors thank the department of Biomedical Engineering and Mechanics at Virginia Tech for partial financial support of BM and the use of its facilities, and Macromolecules and Interfaces Institute at Virginia Tech for fostering interdisciplinary research in adhesion science. The authors are also grateful to the two anonymous reviewers for providing constructive comments and suggestions on an earlier version of the paper that have improved upon the presentation of the work.

Appendix

In the limit of a vanishingly small CZ size, the solution of the present problem can be found by modifying Ghatak et al.'s [8] solution. Using our nondimensionalization of variables and setting $W = w_p/\delta_f$, the ODEs that govern bending of the plate can be written as

$$\text{free region:} \quad (-A \le X < 0) \quad \Lambda^4 W = 0 \tag{A1}$$

$$\text{bonded region:} \quad (X \ge 0) \quad (\Lambda^6 - 1)W = 0 \tag{A2}$$

The solution to Eqs. (A1) and (A2) are, respectively, given as Eqs. (A3) and (A4)

$$W = A_1 X^3 + A_2 X^2 + A_3 X + A_4 \tag{A3}$$

$$\begin{aligned} W(X) &= A_5 e^{-X} + A_6 e^{X} \\ &+ e^{-\frac{X}{2}}\left(A_7 \cos\left(\frac{\sqrt{3}}{2}X\right) + A_8 \sin\left(\frac{\sqrt{3}}{2}X\right)\right) \\ &+ e^{\frac{X}{2}}\left(A_9 \cos\left(\frac{\sqrt{3}}{2}X\right) + A_{10} \sin\left(\frac{\sqrt{3}}{2}X\right)\right) \end{aligned} \tag{A4}$$

Here, $A_1, A_2, ..., A_{10}$ are integration constants. Noting that $\lim_{X\to\infty} W = 0$, one can neglect A_6, A_9, and A_{10}. In order to solve for the remaining seven integration constants, the following seven conditions are used.

Boundary conditions at the plate edge:

$$\begin{aligned} W(-A) &= \Delta_A \\ W''(-A) &= 0 \end{aligned} \tag{A5}$$

Continuity of plate deflection, slope, bending moment, and shear force at the debond tip:

$$\begin{aligned} W(0^-) &= W(0^+) \\ W'(0^-) &= W'(0^+) \\ W''(0^-) &= W''(0^+) \\ W'''(0^-) &= W'''(0^+) \end{aligned} \tag{A6}$$

Debond tip peel stress:

$$\begin{aligned} W''''(0^+) &= -(\eta_e{}^{-2} + \eta_s^{-2})W(0^+) \quad \text{(until damage initiation)} \\ &= -\eta_s^{-2} \quad \text{(after damage initiation)} \end{aligned} \tag{A7}$$

We note that the condition (A7) distinguishes this analysis from Ghatak et al.'s work who assumed that the peel stress had a local maximum at the debond tip and set $W''''(0^+) = 0$. Upon solving for the integration constants and setting $\eta_e \to 0$, the load, P_A, can be found as

$$\text{prior to damage initiation:} \quad P_A = \frac{6\Delta_A}{(3A + 6A^2 + 2A^3)} \tag{A8}$$

$$\text{after damage initiation:} \quad P_A = \frac{3\Delta_A}{(9 + 12A + 6A^2 + A^3)} + \frac{1}{\eta_s^2}\frac{3(2+A)}{(9 + 12A + 6A^2 + A^3)} \tag{A9}$$

A quadratic relation (A10) is found between A and Δ_A upon writing the energy criterion for debond propagation, $-(\partial\bar{u}/\partial a) = \mathcal{G}_c$, where $\bar{u}$ is the strain energy of the system. In terms of our nondimensional variables, it becomes $(\partial U/\partial A) = -(\eta_s^2/2)$ where the dimensionless energy is found as $U = \int_0^{\Delta_A} P d\Delta_A = \int_0^{\Delta_{A1}} P d\Delta_A + \int_{\Delta_{A1}}^{\Delta_A} P d\Delta_A$, where $\Delta_{A1} = (A(3 + 6A + 2A^2)/3(3 + 2A)\eta_s^2)$ is the damage initiation displacement satisfying Eqs. (A8) and (A9)

$$C_1 {\Delta_A}^2 + C_2 \Delta_A + C_3 = 0 \tag{A10}$$

The coefficients, $C_1, ..., C_3$ are given as

$$\begin{aligned} C_1 &= \frac{27(2+A)^2}{\left(1 + (A+2)^3\right)^2}, \quad C_2 = \frac{18\left(1 + 4(A+2)^2\right)}{\left(1 + (A+2)^3\right)^2}, \\ C_3 &= \frac{2(9 + 30A + 18A^2 + 4A^3)}{(3+2A)^3} + 3\eta_s^{-2} \end{aligned} \tag{A11}$$

It can be shown that the second term on the right-hand side (RHS) of Eq. (A9) causes an offset of the predicted LD curve from the LEFM result [8] because it causes a smaller debond length at a given displacement and a slower rate of increase of the debond length as a function of the applied displacement. When the second term on the RHS of Eq. (A9) is disregarded, one obtains Eq. (A12) upon applying the energy criterion for debond propagation

$$\Delta^2 = \frac{\left((A+2)^3 + 1\right)^2}{9\eta_s^2 (A+2)^2} \tag{A12}$$

The $A - \Delta_A$ curves predicted from Eqs. (A10) and (A12) for $\eta_s = 1$ are plotted and compared with the corresponding LEFM predictions, respectively, in Figs. 10(*a*) and 10(*b*). It is clear that results from these two equations are very close to those of Ghatak et al.

References

[1] Kaelble, D., 1959, "Theory and Analysis of Peel Adhesion: Mechanisms and Mechanics," Trans. Soc. Rheol., **3**(1), pp. 161–180.
[2] Kaelble, D., 1960, "Theory and Analysis of Peel Adhesion: Bond Stresses and Distributions," Trans. Soc. Rheol., **4**(1), pp. 45–73.
[3] Bikerman, J., 1957, "Theory of Peeling Through a Hookean Solid," J. Appl. Phys., **28**(12), pp. 1484–1485.
[4] Spies, G., 1953, "The Peeling Test on Redux-Bonded Joints: A Theoretical Analysis of the Test Devised by Aero Research Limited," Aircr. Eng. Aerosp. Technol., **25**(3), pp. 64–70.
[5] Kaelble, D., 1965, "Peel Adhesion: Micro-Fracture Mechanics of Interfacial Unbonding of Polymers," Trans. Soc. Rheol., **9**(2), pp. 135–163.
[6] Dillard, D., 1989, "Bending of Plates on Thin Elastomeric Foundations," ASME J. Appl. Mech., **56**(2), pp. 382–386.
[7] Lefebvre, D. R., Dillard, D. A., and Brinson, H., 1988, "The Development of a Modified Double-Cantilever-Beam Specimen for Measuring the Fracture Energy of Rubber to Metal Bonds," Exp. Mech., **28**(1), pp. 38–44.
[8] Ghatak, A., Mahadevan, L., and Chaudhury, M. K., 2005, "Measuring the Work of Adhesion Between a Soft Confined Film and a Flexible Plate," Langmuir, **21**(4), pp. 1277–1281.

[9] Bao, G., and Suo, Z., 1992, "Remarks on Crack-Bridging Concepts," ASME Appl. Mech. Rev., **45**(8), pp. 355–366.
[10] Xu, X.-P., and Needleman, A., 1996, "Numerical Simulations of Dynamic Crack Growth Along an Interface," Int. J. Fract., **74**(4), pp. 289–324.
[11] Geubelle, P. H., and Baylor, J. S., 1998, "Impact-Induced Delamination of Composites: A 2D Simulation," Compos. Part B: Eng., **29**(5), pp. 589–602.
[12] Dugdale, D., 1960, "Yielding of Steel Sheets Containing Slits," J. Mech. Phys. Solids, **8**(2), pp. 100–104.
[13] Tang, T., and Hui, C. Y., 2005, "Decohesion of a Rigid Punch From an Elastic Layer: Transition From "Flaw Sensitive" to "Flaw Insensitive" Regime," J. Polym. Sci. Part B: Polym. Phys., **43**(24), pp. 3628–3637.
[14] Williams, J., and Hadavinia, H., 2002, "Analytical Solutions for Cohesive Zone Models," J. Mech. Phys. Solids, **50**(4), pp. 809–825.
[15] Georgiou, I., Hadavinia, H., Ivankovic, A., Kinloch, A., Tropsa, V., and Williams, J., 2003, "Cohesive Zone Models and the Plastically Deforming Peel Test," J. Adhes., **79**(3), pp. 239–265.
[16] Blackman, B., Hadavinia, H., Kinloch, A., and Williams, J., 2003, "The Use of a Cohesive Zone Model to Study the Fracture of Fibre Composites and Adhesively-Bonded Joints," Int. J. Fract., **119**(1), pp. 25–46.
[17] Ouyang, Z., and Li, G., 2009, "Local Damage Evolution of Double Cantilever Beam Specimens During Crack Initiation Process: A Natural Boundary Condition Based Method," ASME J. Appl. Mech., **76**(5), p. 051003.
[18] Plaut, R. H., and Ritchie, J. L., 2004, "Analytical Solutions for Peeling Using Beam-on-Foundation Model and Cohesive Zone," J. Adhes., **80**(4), pp. 313–331.
[19] Stigh, U., 1988, "Damage and Crack Growth Analysis of the Double Cantilever Beam Specimen," Int. J. Fract., **37**(1), pp. R13–R18.
[20] Biel, A., and Stigh, U., 2007, "An Analysis of the Evaluation of the Fracture Energy Using the DCB-Specimen," Arch. Mech., **59**(4–5), pp. 311–327.
[21] Dhong, C., and Fréchette, J., 2015, "Coupled Effects of Applied Load and Surface Structure on the Viscous Forces During Peeling," Soft Matter, **11**(10), pp. 1901–1910.
[22] Timoshenko, S., 1940, *Theory of Plates and Shells*, McGraw-Hill, New York.
[23] Ripling, E., Mostovoy, S., and Patrick, R., 1964, "Measuring Fracture Toughness of Adhesive Joints," Mater. Res. Stand., **4**(3), pp. 129–134.
[24] Maugis, D., 1992, "Adhesion of Spheres: the JKR-DMT Transition Using a Dugdale Model," J. Colloid Interface Sci., **150**(1), pp. 243–269.
[25] Reynolds, O., 1886, "On the Theory of Lubrication and Its Application to Mr. Beauchamp Tower's Experiments, Including an Experimental Determination of the Viscosity of Olive Oil," Proc. R. Soc. London, **40**(242–245), pp. 191–203.
[26] Wolfram, Research, 2014, Mathematica, Wolfram Research, Champaign, IL.
[27] Mukherjee, B., Batra, R. C., and Dillard, D. A., 2016, "Effect of Confinement and Interfacial Adhesion on Peeling of a Flexible Plate From an Elastomeric Layer," Int. J. Solids Struct. (in press).
[28] Obreimoff, J., 1930, "The Splitting Strength of Mica," Proc. R. Soc. London A, **127**(805), pp. 290–297.
[29] Ha, K., Baek, H., and Park, K., 2015, "Convergence of Fracture Process Zone Size in Cohesive Zone Modeling," Appl. Math. Model., **39**(19), pp. 5828–5836.
[30] Ghatak, A., 2006, "Confinement-Induced Instability of Thin Elastic Film," Phys. Rev. E, **73**(4), p. 041601.
[31] Ghatak, A., Chaudhury, M. K., Shenoy, V., and Sharma, A., 2000, "Meniscus Instability in a Thin Elastic Film," Phys. Rev. Lett., **85**(20), p. 4329.
[32] Ghatak, A., and Chaudhury, M. K., 2003, "Adhesion-Induced Instability Patterns in Thin Confined Elastic Film," Langmuir, **19**(7), pp. 2621–2631.
[33] Li, S., Wang, J., and Thouless, M., 2004, "The Effects of Shear on Delamination in Layered Materials," J. Mech. Phys. Solids, **52**(1), pp. 193–214.
[34] Ghatak, A., Mahadevan, L., Chung, J. Y., Chaudhury, M. K., and Shenoy, V., 2004, "Peeling From a Biomimetically Patterned Thin Elastic Film," Proc. R. Soc. London Ser. A, **460**(2049), pp. 2725–2735.